J|A|C|S
ARTICLES
Published on Web 05/11/2002

Deuterium Spin Probes of Side-Chain Dynamics in Proteins. 1. Measurement of Five Relaxation Rates per Deuteron in ^{13}C-Labeled and Fractionally ^{2}H-Enriched Proteins in Solution

Oscar Millet, D. R. Muhandiram, Nikolai R. Skrynnikov, and Lewis E. Kay*

Contribution from the Protein Engineering Network Centers of Excellence and Departments of Medical Genetics and Microbiology, Biochemistry, and Chemistry, University of Toronto, Toronto, Ontario, Canada M5S 1A8

Received November 7, 2001. Revised Manuscript Received January 29, 2002

Abstract: New pulse sequences are presented for the measurement of the relaxation of deuterium double quantum, quadrupolar order, and transverse antiphase magnetization in $^{13}CH_2D$ methyl groups of ^{15}N-, ^{13}C-labeled, fractionally deuterated proteins. Together with previously developed experiments for measuring deuterium longitudinal and transverse decay rates [Muhandiram, D. R.; Yamazaki, T.; Sykes, B. D.; Kay, L. E. *J. Am. Chem. Soc.* **1995**, *117*, 11536], these schemes allow measurement of the five unique decay constants of a single deuteron, providing an unprecedented opportunity to investigate side-chain dynamics in proteins. All five deuterium relaxation rates have been measured for deuterons in the methyl groups of the B1 immunoglobulin binding domain of peptostreptococcal protein L and the N-terminal SH3 domain from the protein drk. Since values of the spectral density function at only three different frequencies contribute to the five relaxation rates, the self-consistency of the relaxation data is readily established. Very good agreement is obtained between calculated parameters describing the amplitudes and time scales of motion when different subsets of the relaxation data are employed.

Introduction

Much of protein function is predicated on dynamics. For example, ligand binding,[1,2] enzyme catalysis,[1,3,4] and molecular recognition and signal transduction processes[5] often require a certain level of structural plasticity and flexibility. In addition, molecular dynamics can provide an important contribution to protein stability through increases in the entropy of the system.[6] Protein dynamics have been studied using a variety of biophysical approaches including X-ray diffraction[1], neutron scattering,[7] simulations,[8] and a large number of different spectroscopies.[9−12] NMR spectroscopy is a particularly powerful tool for studying molecular motion since a wide range of time scales, extending from picoseconds to seconds, can be probed by spin relaxation and because dynamic information is available on a per-site basis.[13−15] Studies to date have primarily focused on characterizing backbone dynamics through measurement of ^{15}N spin relaxation parameters at each site in the protein, but more recently experiments have emerged for investigating side-chain motions.[16−24]

In the past several years our laboratory has developed an approach for studying side-chain dynamics in proteins in which ^{2}H spin relaxation is measured in CHD and CH_2D spin systems in ^{13}C-labeled, fractionally deuterated molecules.[18,21] Specifically, by measuring ^{2}H longitudinal (R_1) and transverse ($R_{1\rho}$) relaxation rates, order parameters characterizing the amplitudes of motions and correlation times describing their rates can be obtained. Several recent applications include studies leading to the interpretation of side-chain dynamics in terms of energetics at molecular interfaces in protein−peptide[25−27] and protein−

* Corresponding author. E-mail: kay@bloch.med.utoronto.ca.

(1) Alber, T.; Gilbert, W. A.; Ponzi, D. R.; Petsko, G. A. *Ciba Found. Symp.* **1983**, *93*, 4−24.
(2) Frauenfelder, H.; Sligar, S. G.; Wolynes, P. G. *Science* **1991**, *254*, 1598−1603.
(3) Huber, R. *Trends Biochem. Sci.* **1979**, *4*, 271−276.
(4) Fersht, A. *Enzyme Structure and Mechanism*; 2nd ed.; Freeman & Co.: New York, 1985.
(5) Pawson, T. *Nature* **1995**, *373*, 573−580.
(6) Makhatadze, G. I.; Privalov, P. L. *Adv. Protein Chem.* **1995**, *47*, 307−425.
(7) Zaccai, G. *Science* **2000**, *288*, 1604−1607.
(8) Karplus, M.; McCammon, J. A. *Annu. Rev. Biochem.* **1983**, *53*, 263−300.
(9) Palmer, A. G.; Williams, J.; McDermott, A. *J. Phys. Chem.* **1996**, *100*, 13293−13310.
(10) Dadusc, G.; Ogilvie, J. P.; Schulenberg, P.; Marvet, U.; Miller, R. J. *Proc. Natl. Acad. Sci. U.S.A.* **2001**, *98*, 6110−5.
(11) Hubbell, W. L.; Cafiso, D. S.; Altenbach, C. *Nat. Struct. Biol.* **2000**, *7*, 735−9.
(12) Weiss, S. *Nat. Struct. Biol.* **2000**, *7*, 724−729.
(13) Kay, L. E. *Nat. Struct. Biol. NMR Suppl.* **1998**, *5*, 513−516.
(14) Ishima, R.; Torchia, D. A. *Nat. Struct. Biol.* **2000**, *7*, 740−743.
(15) Palmer, A. G.; Kroenke, C. D.; Loria, J. P. *Methods Enzymol.* **2001**, *339*, 204−238.
(16) Palmer, A. G.; Wright, P. E.; Rance, M. *Chem. Phys. Lett.* **1991**, *185*, 41−46.
(17) Kay, L. E.; Bull, T. E.; Nicholson, L. K.; Griesinger, C.; Schwalbe, H.; Bax, A.; Torchia, D. A. *J. Magn. Reson.* **1992**, *100*, 538−558.
(18) Muhandiram, D. R.; Yamazaki, T.; Sykes, B. D.; Kay, L. E. *J. Am. Chem. Soc.* **1995**, *117*, 11536−11544.
(19) LeMaster, D. M.; Kushlan, D. M. *J. Am. Chem. Soc.* **1996**, *118*, 9255−9264.
(20) Lee, A. L.; Urbauer, J. L.; Wand, A. J. *J. Biomol. NMR* **1997**, *9*, 437−440.
(21) Yang, D.; Mittermaier, A.; Mok, Y. K.; Kay, L. E. *J. Mol. Biol.* **1998**, *276*, 939−954.
(22) Ishima, R.; Louis, J. M.; Torchia, D. A. *J. Am. Chem. Soc.* **1999**, *121*, 1, 11589−11590.
(23) Mulder, F. A. A.; Skrynnikov, N. R.; Hon, B.; Dahlquist, F. W.; Kay, L. E. *J. Am. Chem. Soc.* **2000**, *123*, 967−975.
(24) Skrynnikov, N. R.; Mulder, F. A. A.; Hon, B.; Dahlquist, F. W.; Kay, L. E. *J. Am. Chem. Soc.* **2001**, *123*, 4556−4566.

nucleic acid[28] systems and investigations of the origin of differences in binding between structurally homologous proteins.[29] A very elegant temperature dependent study of internal dynamics in calmodulin shows a heterogeneous distribution of entropy in the molecule and provides insight into the microscopic origins of heat capacity in proteins.[30]

Despite the growing number of studies that have focused on side-chain motions in proteins, our understanding of their dynamics remains incomplete and it would be helpful to have additional experiments to complement the ^{2}H R_1 and $R_{1\rho}$ measurements that have been used to date. The deuteron is a particularly powerful probe in this regard since for an isolated spin there are five elements of the density matrix (or linear combinations thereof) that relax independently and hence five unique relaxation rates are available.[31] Two of the five linear combinations are proportional to longitudinal and transverse magnetization and these modes relax with the rates R_1 and $R_{1\rho}$ mentioned above. Pioneering studies of Vega and Pines,[32] Luz and co-workers,[33] and later Bodenhausen et al.[34] led to the development of methods to excite an additional mode, ^{2}H double quantum coherence, in molecules that are oriented. Subsequently Yen and Weitekamp showed that remarkably it is possible to create double quantum coherence in spin-1 systems even in the case where such spins are attached to molecules in isotropic solution.[35] Building on these important developments, we present here an experiment for measuring deuterium double quantum relaxation in fractionally deuterated, ^{13}C-labeled proteins in isotropic solution. In addition, related pulse schemes are presented for obtaining relaxation rates of the remaining two independent modes, ^{2}H quadrupolar order and antiphase transverse magnetization. The methodology focuses on using methyl groups as probes of dynamics, since as discussed previously,[18,36] methyls are in general well-dispersed in proteins, are often present at molecular interfaces, and have favorable spectroscopic properties. In the first of a series of two papers the methodology for measuring the three additional rates described above is discussed. Subsequently, we demonstrate in two different protein systems, at different temperatures, and with data recorded at a number of different spectrometer fields that the five relaxation rates measured per methyl site are internally consistent. An analysis of the relaxation data recorded on the 63 residue B1 immunoglobulin binding domain of peptostreptococcal protein L[37] in terms of parameters reflecting the amplitude and time scale of side-chain motion is shown to be consistent with analyses based exclusively on using R_1 and $R_{1\rho}$ rates. In the following paper in this issue an in-depth analysis of the relaxation data in terms of molecular dynamics is presented.

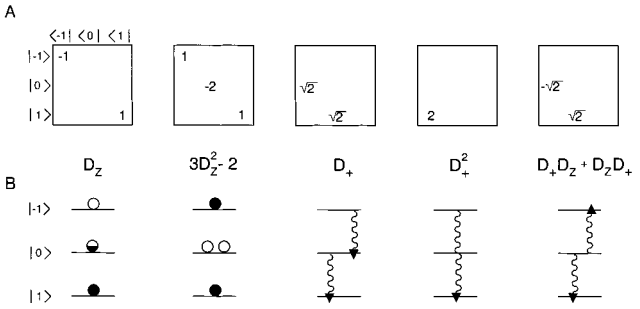

Figure 1. The five independent operators for an isolated ^{2}H spin describing longitudinal magnetization D_Z, quadrupolar order $3D_Z^2 - 2$, single quantum in-phase coherence D_+, double quantum coherence D_+^2, and single quantum antiphase coherence $D_+D_Z + D_ZD_+$. (A) Matrix representation of the operators, with only nonzero elements displayed. (B) Schematic representation of the basis operators in the context of energy levels. For the spin orders overpopulated states are represented by filled circles and depleted states by open circles. A half-filled bead is used for a state with no excess population relative to a demagnetized saturated state. In the case of the three coherences, D_+, D_+^2, and $D_+D_Z + D_ZD_+$, the corresponding transitions are depicted by wavy lines with arrowheads.

Results and Discussion

Relaxation of Deuterium. The density matrix of a spin-1 particle can be written as a linear combination of five independent operators, in addition to the identity operator, that relax with distinct rates.[31] Figure 1A shows the matrix representation for these five operators (only nonzero matrix elements are indicated) with D_Z and $D_+ = D_X + iD_Y$ representing longitudinal and transverse components of the density operator, respectively. Both operators D_Z (longitudinal magnetization) and $3D_Z^2 - 2$ (quadrupolar order) are related to populations of states, while the remaining three terms, D_+ (in-phase transverse magnetization), $D_+D_Z + D_ZD_+$ (antiphase transverse magnetization), and D_+^2 (double quantum magnetization) correspond to transitions between spin states. This is indicated schematically in Figure 1B. The expressions describing the relaxation of these five modes are given by[31]

$$R^Q(D_Z) = \frac{3}{40}\left(\frac{e^2qQ}{\hbar}\right)^2[J(\omega_D) + 4J(2\omega_D)] \quad (1a)$$

$$R^Q(3D_Z^2 - 2) = \frac{3}{40}\left(\frac{e^2qQ}{\hbar}\right)^2[3J(\omega_D)] \quad (1b)$$

$$R^Q(D_+) = \frac{1}{80}\left(\frac{e^2qQ}{\hbar}\right)^2[9J(0) + 15J(\omega_D) + 6J(2\omega_D)] \quad (1c)$$

$$R^Q(D_+D_Z + D_ZD_+) = \frac{1}{80}\left(\frac{e^2qQ}{\hbar}\right)^2[9J(0) + 3J(\omega_D) + 6J(2\omega_D)] \quad (1d)$$

$$R^Q(D_+^2) = R^Q(D_X^2 - D_Y^2) = \frac{3}{40}\left(\frac{e^2qQ}{\hbar}\right)^2[J(\omega_D) + 2J(2\omega_D)] \quad (1e)$$

where (e^2qQ/h) is the quadrupolar coupling constant and $J(\omega)$ is a spectral density function containing the dynamics information. A number of different motional models can be used to

(25) Kay, L. E.; Muhandiram, D. R.; Farrow, N. A.; Aubin, Y.; Forman-Kay, J. D. *Biochemistry* **1996**, *35*, 361−368.
(26) Kay, L. E.; Muhandiram, D. R.; Wolf, G.; Shoelson, S. E.; Forman-Kay, J. D. *Nat. Struct. Biol.* **1998**, *5*, 156−163.
(27) Lee, A. L.; Kinnear, S. A.; Wand, A. J. *Nat. Struct. Biol.* **2000**, *7*, 72−77.
(28) Mittermaier, A.; Varani, L.; Muhandiram, D. R.; Kay, L. E.; Varani, G. *J. Mol. Biol.* **1999**, *294*, 967−79.
(29) Constantine, K. L.; Friedrichs, M. S.; Wittekind, M.; Jamil, H.; Chu, C. H.; Parker, R. A.; Goldfarb, V.; Mueller, L.; Farmer, B. T. *Biochemistry* **1998**, *37*, 7965−7980.
(30) Lee, A. L.; Wand, A. J. *Nature* **2001**, *411*, 501−504.
(31) Jacobsen, J. P.; Bildsoe, H. K.; Schaumburg, K. *J. Magn. Reson.* **1976**, *23*, 153−164.
(32) Vega, S.; Pines, A. *J. Chem. Phys.* **1977**, *66*, 5624−5644.
(33) Hsi, S.; Zimmerman, H.; Luz, Z. *J. Chem. Phys.* **1978**, *69*, 4126−4146.
(34) Bodenhausen, G.; Vold, R. L.; Vold, R. R. *J. Magn. Reson.* **1980**, *37*, 93−106.
(35) Yen, Y. S.; Weitekamp, D. P. *J. Magn. Reson.* **1982**, *47*, 476−482.
(36) Gardner, K. H.; Rosen, M. K.; Kay, L. E. *Biochemistry* **1997**, *36*, 1389−1401.
(37) Scalley, M. L.; Yi, Q.; Gu, H.; McCormack, A.; Yates, J. R.; Baker, D. *Biochemistry* **1997**, *36*, 3373−82.

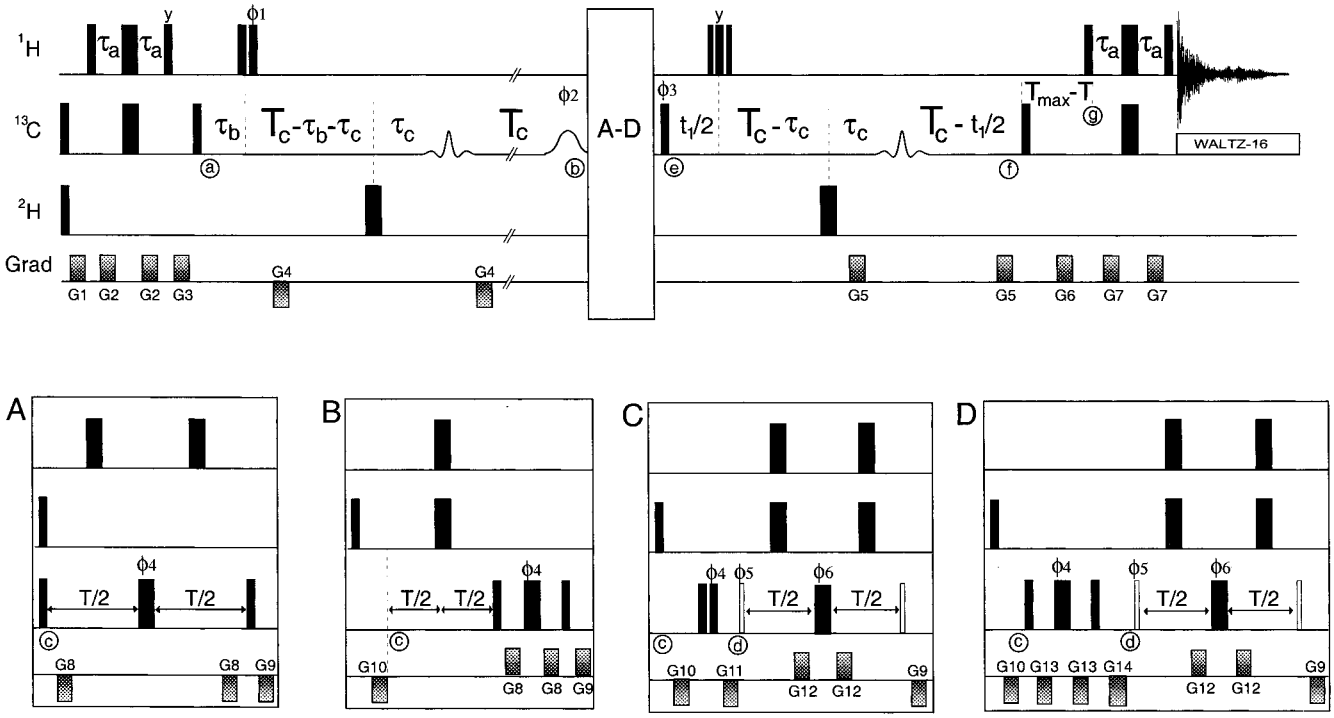

Figure 2. Pulse schemes for the measurement of deuterium relaxation rates $R^Q(D_+{}^2)$, $R^Q(3D_Z{}^2 - 2)$, and $R^Q(D_+D_Z + D_ZD_+)$ in $^{13}CH_2D$ spin systems. These experiments are complementary to the ones illustrated in Figure 6 of Muhandiram et al.[18] for measuring $R^Q(D_Z)$ and $R^Q(D_+)$. Blocks A and B are inserted into the scheme for measurement of $R^Q(D_+{}^2)$ and $R^Q(3D_Z{}^2 - 2)$, respectively, while either block C or D can be used for measurement of $R^Q(D_+D_Z + D_ZD_+)$. All narrow (wide) rectangular pulses correspond to flip angles of 90° (180°) and are applied along the *x*-axis unless otherwise indicated. The narrow rectangular pulses that are not filled in blocks C and D have flip angles of 45°. ^{1}H pulses (32 kHz field) are centered at 1 ppm until prior to point *g*, at which time the carrier is jumped to 4.7 ppm. ^{13}C and ^{2}H rectangular pulses are centered at 20 and 0.8 ppm, respectively, and are applied using 18.5 and 1.9 kHz fields. The shaped carbon 180° pulses (REBURP[51]), applied in the middle of the periods extending from points *a* to *b* and *e* to *f* are of duration 360 μs (600 MHz field), with the center of excitation shifted to 42 ppm via phase modulation of the rf field.[52,53] The 90° ^{13}C selective pulse applied at point *b* has the SEDUCE-1 profile,[54] a duration of 655 μs (600 MHz), and is centered at 57.5 ppm. Decoupling during acquisition is achieved using a 2.3 kHz WALTZ-16 sequence.[55] The delays employed are as follows: $\tau_a = \tau_c = 1.7$ ms, $\tau_b = 3.85$ ms, and $T_C = 14.5$ ms. Duration and strength of the gradients are as follows (with the sign of the gradients indicated in the figure): G1, 0.5 ms, 5 G/cm; G2, 0.3 ms, 3 G/cm; G3, 1.5 ms, 15 G/cm; G4, 0.3 ms, 25 G/cm; G5, 0.2 ms, 10 G/cm; G6, 1.0 ms, 15 G/cm; G7, 0.3 ms, 2 G/cm; G8, 0.4 ms, 10 G/cm; G9, 0.3 ms, 5 G/cm; G10, 0.4 ms, 7 G/cm; G11, 0.2 ms, 12 G/cm; G12, 0.05 ms, 25 G/cm; G13, 0.4 ms, 10 G/cm; G14, 0.2 ms, 12G/cm. To ensure that the effects of gradients G4, G5, and G6 and all the gradients inside blocks A−C are additive with respect to dephasing of water, the sign of these gradients is changed in concert with alternation of the rf phase $\phi1$, as described previously.[18] Note that, in this regard, for scheme B the sign of the gradients G5 and G6 must be reversed relative to what is shown in the figure. Phase cycle: $\phi1 = (x, -x)$; $\phi2 = 4(x),4(-x)$; $\phi3 = 2(x), 2(-x)$. In the case of schemes A and B, $\phi4 = 4(0°),4(45°),4(90°),4(135°)$; Rec = $x,2(-x),x,-x,2(x),-x$. Scheme C, $\phi4 = 4(x),4(-x)$; $\phi5 = 8(x),8(-x)$; $\phi6 = 2(x),2(-x)$; Rec = $x,2(-x),2(x),2(-x),x,-x,2(x),2(-x),2(x),-x$. Scheme D, $\phi4 = 2(0°),2(90°),2(45°),2(135°)$; $\phi5 = 8(x),8(-x)$; $\phi6 = 2(x),2(-x)$; Rec = $x,2(-x),x,-x,2(x),2(-x),2(x),-x,x,2(-x),x$. Quadrature in F_1 is achieved via States-TPPI of $\phi3$.[56]

describe the dynamics of methyl groups in proteins. In this paper we have used a simple form,[38,39]

$$J(\omega) = \alpha S_f{}^2 \frac{\tau_R}{1 + (\omega\tau_R)^2} + (1 - \alpha S_f{}^2) \frac{\tau}{1 + (\omega\tau)^2} \quad (2)$$

with more complex models considered on a case by case basis in the subsequent paper. In eq 2 τ_R is the (assumed isotropic) overall tumbling correlation time, $\tau^{-1} = \tau_R{}^{-1} + \tau_f{}^{-1}$, where τ_f is a correlation time for the fast internal motion(s), $S_f{}^2$ describes the amplitude of fast local motion of the 3-fold symmetry axis of the methyl group and $\alpha = (3\cos^2\theta - 1)^2/4$, where θ is the angle between the C−D bond and the symmetry axis (109.5°).[40] Note that this form of spectral density (eq 2) can also be used when other relaxation interactions are considered and in this case α can take on different values (see Materials and Methods). It is clear from inspection of eq 1 that the relaxation of the five independent deuterium spin modes depends exclusively on spectral densities evaluated at the three distinct frequencies, 0, ω_D, and $2\omega_D$, where ω_D is the deuterium Larmor frequency. Measurement of the five rates listed in eq 1 therefore allows one to determine the three values of the spectral density, $J(0)$, $J(\omega_D)$ and $J(2\omega_D)$ without any a priori assumptions about the magnitude of these terms.

Pulse Sequences for ^{2}H Relaxation Measurements. Figure 2 illustrates the pulse sequences that have been developed for measurement of the ^{2}H relaxation rates $R^Q(D_+{}^2) = R^Q(D_X{}^2 - D_Y{}^2)$ (scheme A), $R^Q(3D_Z{}^2 - 2)$ (scheme B), and $R^Q(D_+D_Z + D_ZD_+) = R^Q(D_XD_Z + D_ZD_X) = R^Q(D_YD_Z + D_ZD_Y)$ (schemes C, D). (Note that in what follows $R^Q(D_+{}^2)$ and $R^Q(D_X{}^2 - D_Y{}^2)$ will be used interchangeably.) The experiments are closely related to pulse sequences for measuring $R^Q(D_Z)$ and $R^Q(D_+)$ (see Figure 6 of Muhandiram et al.[18]) that have been presented previously and only a brief overview of the schemes are therefore given, with particular focus on the insets A−D in the figure. At point *a* in the scheme the signal of interest is of the form, I_ZC_Y, where *I* and *C* denote proton and carbon magnetization, respectively. The preparation period extending from *a* to *b* is set to $1/J_{CC}$, so that evolution due to the one-bond ^{13}C−^{13}C scalar coupling, J_{CC}, is refocused. During this interval methyl

(38) Lipari, G.; Szabo, A. *J. Am. Chem. Soc.* **1982**, *104*, 4559−4570.
(39) Lipari, G.; Szabo, A. *J. Am. Chem. Soc.* **1982**, *104*, 4546−4559.
(40) Mittermaier, A.; Kay, L. E. *J. Am. Chem. Soc.* **1999**, *121*, 10608−10613.

isotopomers of the form $^{13}CH_2D$ are selected by the $90_x90_{\phi 1}$ pulse pair applied after the delay τ_b following point *a* (see ref 18). At the heart of the experiments is the evolution of ^{13}C magnetization that occurs during this period (*a* to *b*) due to the one-bond $^{13}C-^2H$ scalar coupling. The terms at point *b* which derive from this evolution and which contribute ultimately to the signal of interest are given by the expression

$$I_Z C_Y(1 - D_Z^2) + I_Z C_Y D_Z^2 \cos[2\pi J_{CD}(2T_C - 2\tau_C)] - I_Z C_X D_Z \sin[2\pi J_{CD}(2T_C - 2\tau_C)] \quad (3)$$

The first term in eq 3 corresponds to magnetization derived from the central line of the ^{13}C triplet which does not evolve with respect to the one bond $^{13}C-^2H$ scalar coupling, J_{CD}. The second and third terms represent ^{13}C magnetization from the outer lines of the triplet that are either in-phase or antiphase with respect to the ^2H spin, *D*. The delay τ_C is chosen so that $2T_C - 2\tau_C = 1/2J_{CD}$, and only the first two terms in eq 3 contribute, therefore, to the observed signal. The third term would be eliminated in any event as a result of double quantum filters or purging pulses that are applied subsequently in the pulse sequence (see below). Note that at this point in the scheme ^{13}C magnetization has been created in which the inner and outer lines are 180°out of phase, $I_Z C_Y(1 - D_Z^2) - I_Z C_Y D_Z^2$. This nonequilibrium state can subsequently be manipulated in different ways (boxes A−D) to obtain the relaxation rates of the desired operators $D_X^2 - D_Y^2$, $3D_Z^2 - 2$, and $D_+D_Z + D_ZD_+$.

Focusing on box A for the moment, at point *c* the magnetization is given by $I_Z C_Z(1 - D_Y^2) - I_Z C_Z D_Y^2 = I_Z C_Z + I_Z C_Z(D_X^2 - D_Y^2) - I_Z C_Z(D_X^2 + D_Y^2)$. During the subsequent interval of duration *T*, ^2H double quantum magnetization, $D_X^2 - D_Y^2$, is selected by phase cycling $\phi 4$ in steps of 45° with inversion of the receiver phase for every 45° increment. Note that when $\phi 4$ is incremented from 0° to 45°, $I_Z C_Z(D_X^2 - D_Y^2)$ changes sign, while $I_Z C_Z$ and $I_Z C_Z(D_X^2 + D_Y^2)$ do not and the desired term can therefore be selected in a straightforward manner. During the variable period *T* evolution of the operator of interest, $I_Z C_Z(D_X^2 - D_Y^2)$, proceeds under the influence of both the ^2H chemical shift and the one-bond $^{13}C-^2H$ coupling ($J_{CD} \sim 20$ Hz) Hamiltonians. Both of these effects are refocused at the end of the period so that $I_Z C_Z(D_X^2 - D_Y^2)$ is retained. However, during *T* the operators $I_Z C_Z(D_X^2 - D_Y^2)$ and $I_Z(D_XD_Y + D_YD_X)$ interconvert (due to J_{CD}), so that the effective relaxation rate of the term of interest is given by

$$R_{\text{eff}} = R(I_Z C_Z D_+^2) - \frac{\Delta}{2}\left(1 - \frac{\sin(2\pi J_{CD}T)}{2\pi J_{CD}T}\right) \quad (4)$$

where $\Delta = R(I_Z C_Z D_+^2) - R(I_Z D_+^2)$, $R(I_Z C_Z D_+^2) = R(I_Z C_Z\{D_X^2 - D_Y^2\})$, and $R(I_Z D_+^2) = R(I_Z\{D_XD_Y + D_YD_X\})$.

Note that R_{eff} is itself a function of *T*, i.e., the decay of $I_Z C_Z(D_X^2 - D_Y^2)$ as a function of *T* is nonexponential. However, because $R(I_Z C_Z D_+^2) \gg \Delta/2$, the second term of eq 4 will make only a very small contribution to the measured rate and can be readily accounted for (see below).

During the interval extending from *e* to *f* in the sequence of Figure 1, ^{13}C chemical shift is recorded and the magnetization transferred to observable signal by way of the reverse of the pathway described above. A set of two-dimensional $^{13}C-^1H$ correlation spectra are obtained as a function of the delay *T*, from which $R^Q(D_+^2) = R^Q(D_X^2 - D_Y^2)$ is extracted (described below). As a final point, it should be noted that prior to the last INEPT transfer when the magnetization of interest is of the form $I_Z C_Z$, a delay of duration $T_{\max} - T$ is inserted between points *f* and *g*, with $T_{\max}$ chosen equal to the maximum value of *T* that is used in the relaxation series. Thus, the effective relaxation rate is given by[41]

$$R_{\text{eff}} = R(I_Z C_Z D_+^2) - \frac{\Delta}{2}\left(1 - \frac{\sin(2\pi J_{CD}T)}{2\pi J_{CD}T}\right) - R(I_Z C_Z) \quad (5)$$

To measure the decay of quadrupolar order the scheme indicated in box B is employed. At point *c* the magnetization is proportional to $I_Z C_Z(1 - D_Z^2) - I_Z C_Z D_Z^2$, and during the subsequent interval of duration *T* these terms relax. Magnetization that is of the form $I_Z C_Z D_Z^2$ is selected by the double quantum filter that follows and then transferred back to observable proton signal in the same manner as described above. The effective relaxation rate that is measured by fitting cross-peak intensities in a series of 2D $^{13}C-^1H$ correlation maps recorded as a function of *T* is given by

$$R_{\text{eff}} = R(I_Z C_Z\{2D_Z^2 - 1\}) - R(I_Z C_Z) \quad (6)$$

with the second term in eq 6 the result of the relaxation delay between points *f* and *g*, as discussed above. It is worth noting that while quadrupolar order is represented by the traceless tensor $3D_Z^2 - 2$, what is measured in the scheme of Figure 1B is the decay of a term proportional to $2D_Z^2 - 1$, eq 6. The dominant contribution to the decay of either terms results from the quadrupolar interaction, and this contribution is the same for both modes (see below).

The decay of antiphase transverse deuterium magnetization can be measured using either scheme C or D in the figure. In the case of scheme C, the ^2H $90_x90_{\phi 4}$ pulse pair after point *c*, where $\phi 4$ is phase cycled $\pm x$ with no inversion of the receiver phase, ensures that residual magnetization of the form $I_Z C_Z D_Z$ is not transferred to observable signal. At point *d* the operators of interest are given by $I_Z C_Z(1 - D_Z^2) - I_Z C_Z D_Z^2$ (see eq 3) and subsequent application of a ^2H 45° pulse generates the desired coherence $I_Z C_Z(D_YD_Z + D_ZD_Y)$, with other terms eliminated by phase cycling. The effective relaxation rate

$$R_{\text{eff}} = R(I_Z C_Z\{D_+D_Z + D_ZD_+\}) - R(I_Z C_Z) \quad (7)$$

is measured from the decay of cross-peak intensities as described above. Scheme D is similar to C except that a double quantum filter is applied to select the term of interest, $I_Z C_Z D_Z^2$, prior to the creation of $I_Z C_Z(D_YD_Z + D_ZD_Y)$. The basic difference between schemes C and D, therefore, is that in C operators that are not desired are selected against, while in D operators of interest are selected for.

Experimental ^2H Relaxation Rates Probe Quadrupolar Relaxation. In a previous series of papers we showed that ^2H longitudinal and transverse relaxation rates, $R^Q(D_Z)$ and $R^Q(D_+)$, could be obtained to excellent approximation by taking the differences $R(I_Z C_Z D_Z) - R(I_Z C_Z)$ and $R(I_Z C_Z D_+) - R(I_Z C_Z)$, respectively.[18,42] In effect, because the ^2H relaxation is so much more efficient than the relaxation of spins *I* and *C* of the methyl

(41) Akke, M.; Palmer, A. G. *J. Am. Chem. Soc.* **1996**, *118*, 911−912.
(42) Yang, D.; Kay, L. E. *J. Magn. Reson. Ser. B* **1996**, *110*, 213-218.

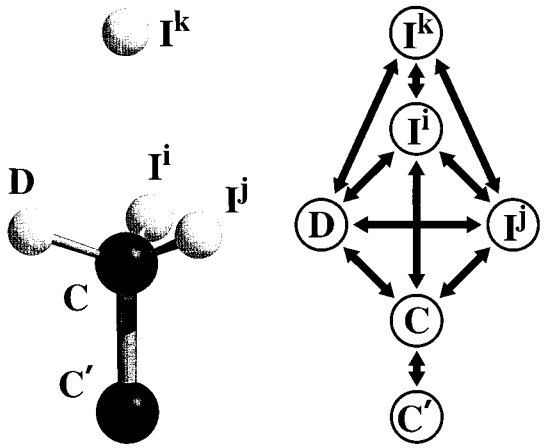

Figure 3. Illustration of the spin system considered in the derivation of the relaxation equations of the Appendix. The dipolar relaxation interactions that are included in the Appendix are indicated by arrows connecting the appropriate pairs of spins.

group, contributions from the quadrupolar interaction can be separated from dipolar contributions involving the other spins. An in-depth analysis also showed that cross-correlation effects are negligible.[42] In what follows we show that it is possible to obtain accurate values for $R^Q(3D_Z^2 - 2)$, $R^Q(D_+D_Z + D_ZD_+)$, and $R^Q(D_+^2) = R^Q(D_X^2 - D_Y^2)$ as well.

Following along the lines of our previous papers,[18,42] we have considered the relaxation contributions to each of I_ZC_Z, $I_ZC_ZD_Z$, $I_ZC_ZD_+$, $I_ZC_Z(2D_Z^2 - 1)$, $I_ZC_Z(D_+D_Z + D_ZD_+)$, and $I_ZC_ZD_+^2$ from dipolar and quadrupolar interactions. Specifically, we can write these contributions as arising from a relaxation Hamiltonian, H^R,

$$H^R = H^Q(D) + H^D(CD) + H^D(I^iD) + H^D(I^jD) + H^D(I^iC) + H^D(I^jC) + H^D(CC') + H^D(I^iI^j) + \sum_{k\neq i,j} H^D(I^iI^k) + \sum_{k\neq i,j} H^D(I^jI^k) + \sum_{k\neq i,j} H^D(DI^k) \quad (8)$$

where H^Q and H^D are contributions from quadrupolar and dipolar interactions, respectively, I^i, I^j, D, and C are the methyl proton, deuteron, and carbon spins, respectively, and C' is the carbon adjacent to the methyl carbon. The summation in the last three terms is over all proton spins k, I^k, that are proximal to the methyl hydrogens. Figure 3 illustrates all of the dipolar contributions that are included in eq 8. In Table 1 of the Appendix we have summarized the contributions to the autorelaxation of the set of six operators, $\{I_ZC_Z, I_ZC_ZD_Z, I_ZC_ZD_+, I_ZC_Z(2D_Z^2 - 1), I_ZC_Z(D_+D_Z + D_ZD_+)$, and $I_ZC_ZD_+^2\}$, where $I_Z = I_Z{}^i + I_Z{}^j$. Using these results, along with eqs 1 and 2, we have established that the equalities

$$\begin{aligned} R(I_ZC_ZD_Z) - R(I_ZC_Z) &\approx R^Q(D_Z) \\ R(I_ZC_ZD_+) - R(I_ZC_Z) &\approx R^Q(D_+) \\ R(I_ZC_Z\{2D_Z{}^2 - 1\}) - R(I_ZC_Z) &\approx R^Q(3D_Z{}^2 - 2) \\ R(I_ZC_Z\{ D_+D_Z + D_ZD_+\}) - R(I_ZC_Z) &\approx R^Q(D_+D_Z + D_ZD_+) \end{aligned} \quad (9)$$

are fulfilled to better than 2% for values of τ_R extending between 3 and 25 ns, S_f^2 between 0.1 and 1.0, $0 \leq \tau_f \leq 150$ ps, and magnetic field strengths extending from 400 to 800 MHz. In the analysis we have also included contributions from external protons I^k, calculated on the basis of the X-ray structure of protein L.[43] Calculations show that these protons can be modeled by including only a single proton at a distance of 2.0 Å from the methyl protons, I^i, I^j, with the resulting relaxation rate attenuated by a factor of 2 to take into account the fact that the protein is 50% deuterated. On the basis of results of the simulations, we have therefore used the rates indicated by the expressions on the left-hand side of eq 9 as excellent approximations to the pure quadrupolar decay rates.

Obtaining values for $R^Q(D_+^2) = R^Q(D_X^2 - D_Y^2)$ is slightly more complex. Equation 4 indicates that the decay of $I_ZC_ZD_+^2$ is complicated by evolution from J_{CD} coupling during the variable interval T. It is clear from eq 4 that the effect of the exchange between operators of the form $I_ZC_ZD_+^2$ and $I_ZD_+^2$ is to decrease the effective decay rate that is measured, since $\Delta \geq 0$. Simulations using the same range of τ_R, S_f^2, and τ_f as listed above indicate that $R(I_ZC_ZD_+^2)$ and $\Delta/2$ differ by at least a factor of 45, and it is therefore not possible to observe deviations from exponential behavior in plots of intensity as a function of T. Nevertheless further simulations using the same T values as employed in experiments establish that there is a systematic (and quite uniform) decrease in measured rates between 2 and 3% over the same range of motional parameters as examined above. We have therefore multiplied all measured values by 1.025 prior to analysis, and these corrected rates very closely approximate $R(I_ZC_ZD_+^2) - R(I_ZC_Z)$ (see eq 5).

Inspection of the relaxation expressions in the Appendix shows that

$$R(I_ZC_ZD_+{}^2) - R(I_ZC_Z) \approx R^Q(D_+{}^2) + 8d_{I^iD}J_{I^iD}(0) + 8d_{I^jD}J_{I^jD}(0) + 8d_{CD}J_{CD}(0) + \sum_{k\neq i,j} R^D_{DI^k} \quad (10)$$

Here $d_{qq'} = (1/10)(\mu_0/4\pi)^2(\hbar\gamma_q\gamma_{q'}/\langle r_{qq'}{}^3\rangle)^2$, γ_q is the gyromagnetic ratio of spin q, $r_{qq'}$ is the distance between spins q and q', h is Plank's constant ($\hbar = h/2\pi$), and $R^D_{DI^k} = 8d_{DI^k}J_{DI^k}(0)$. The sum over k extends to all proximal external protons and the spectral densities $J_{qq'}(0)$ are labeled according to the type of dipolar interaction (I^i-D, I^j-D, I^k-D, or $C-D$) to account for the different geometrical factors that are introduced due to the different orientations of the dipolar vectors with respect to the methyl averaging axis (α of 1/4, 1/4, ~1, and 1/9 for I^i-D, I^j-D, I^k-D, and $C-D$ interactions, respectively; see eq 2). The spectral densities $J_{I^{i,j}D}(0)$ and $J_{CD}(0)$ are, to excellent approximation, the same as the $J(0)$ values that derive from the quadrupolar interaction (aside from a geometrical factor that is necessary for the former term, $J_{I^{i,j}D}(0) \approx (9/4)J_{CD}(0)$; see eq 2), and thus these dipolar terms introduce no additional spectral densities.

It is noteworthy that only in the case of the relaxation of ^{2}H double quantum coherence must these $J(0)$ dipolar contributions be explicitly taken into account. In this case the quadrupolar interaction contributes terms of the form $J(\omega_D)$ and $J(2\omega_D)$ which decrease with increasing molecular size (see eq 1). On the other hand the I−D and C−D dipolar contributions include the dominant $J(0)$ term which increases linearly with size (see eq 10). Simulations indicate for example that for $\tau_R = 4$ ns, $S_f^2 = 0.5$, and $\tau_f = 35$ ps the $J_{I^{i,j}D}(0)$ and $J_{CD}(0)$ terms contribute

(43) O'Neill, J. W.; Kim, D. E.; Baker, D.; Zhang, K. Y. J. *Acta Crystallogr.* **2001**, *D57*, 480−487.

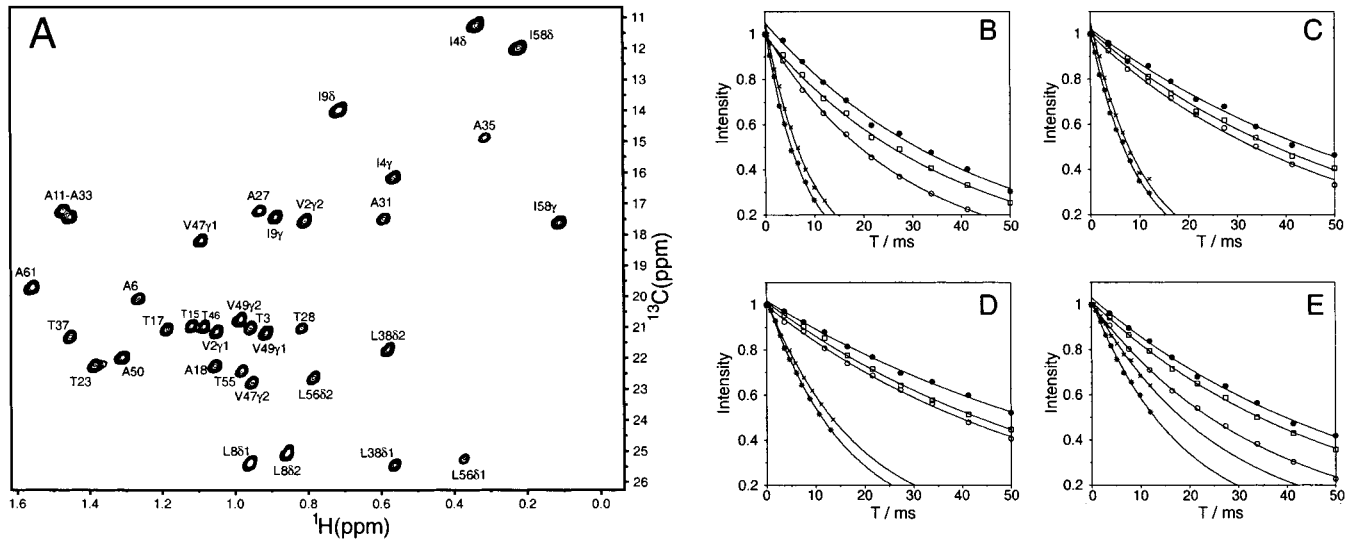

Figure 4. (A) $^{13}C-^{1}H$ HSQC correlation map of the methyl region of the B1 domain of peptostreptococcal protein L recorded at 600 MHz, 298 K, using the scheme of Figure 2A with $T = 1.40$ ms. Note that only signals from methyl groups are observed in this spectrum. The stereospecific assignments of the methyls are indicated. (B−E) Decay curves for the five independent ^{2}H magnetization modes in selected residues: (B) Ala50, (C) Thr17, (D) Ile4γ, and (E) L56δ2 of protein L, 298 K, 600 MHz. In all plots, points correspond to (○) $R^Q(D_Z)$, (∗) $R^Q(D_+)$, (□) $R^Q(3D_Z^2 - 2)$, (●) $R^Q(D_+^2)$, and (×) $R^Q(D_+D_Z + D_ZD_+)$.

approximately 5% to $R(I_ZC_ZD_+^2) - R(I_ZC_Z)$ in total, and this increases to ∼12% for $\tau_R = 10$ ns.

The final term in eq 10, $\sum_{k\neq i,j} R^D_{DI^k}$, includes contributions to the relaxation of the methyl deuteron from all proximal proton spins outside the methyl group in question. Simulations establish that this term is on the order of 1.5−2% (4−5%) of $R^Q(D_+^2)$ for a τ_R value of 4 (10) ns and it is therefore important that these contributions be taken into account. In principle, if the structure of the protein were known to high accuracy and the level of deuteration at each position throughout the molecule could be quantified, it might be possible to obtain an analytical correction factor for each methyl site. However, since the structure and site-specific deuteration content may be unavailable and since the correction is dependent upon side-chain dynamics (which is what we are after in the first place), we prefer to perform a correction for each residue based on experimental data in the following manner. Using measured $R^Q(D_Z)$ and $R^Q(D_+)$ rates along with the τ_R value obtained from ^{15}N spin relaxation data, S_f^2 and τ_f values are obtained on a per-methyl basis, as described by Muhandiram et al.[18] These values are then used to calculate all the terms involved in the relaxation of I_ZC_Z indicated in the Appendix, with the exception of the contributions from external protons. Subtraction of the calculated rate from the measured value for $R(I_ZC_Z)$ provides an excellent estimate of $\sum_{k\neq i,j} R^D_{I^k}$ for a given methyl and $\sum_{k\neq i,j} R^D_{DI^k}$ is readily obtained by multiplication of this value by (γ_D^2/γ_H^2). We found that for protein L at 25 °C ($\tau_R = 4.05$ ns) $\sum_{k\neq i,j} R^D_{DI^k} = 0.55 \pm 0.12$ s^{-1} for the 35 methyls considered (approximately 2.9% of $R^Q(D_+^2)$). Finally, simulations covering the same range of τ_R, S_f^2, and τ_f values as before and including external protons (see above) have established that

$$R(I_ZC_ZD_+^2) - R(I_ZC_Z) - 8d_{I^iD}J_{I^iD}(0) - 8d_{I^jD}J_{I^jD}(0) - 8d_{CD}J_{CD}(0) - \sum_{k\neq i,j} R^D_{DI^k} \approx R^Q(D_+^2) \quad (11)$$

is fulfilled to within 0.5%.

Note that the dipolar corrections such as described above for the relaxation of $I_ZC_ZD_+^2$ are negligible for all other modes, eq 9. In the case of the relaxation of quadrupolar order and longitudinal magnetization, the contributions from $I^{i,j}-D$ and $C-D$ dipolar interactions are less than 0.5% of the pure quadrupolar rate (for both τ_R of 4 and 10 ns) since there are no $J(0)$ terms arising from dipolar interactions. For the in-phase and antiphase transverse terms, D_+ and $D_+D_Z + D_ZD_+$, $J(0)$ dipolar contributions are much smaller than the $J(0)$ quadrupolar terms and again contribute no more than 0.5% to the net relaxation rates (for both $\tau_R = 4$, 10 ns).

We have also considered the effects of cross-correlated spin relaxation between the different relaxation interactions that exist within the framework of the spin network listed in eq 8 and illustrated in Figure 3 and find that they can be neglected. This result is consistent with what we have shown previously in a detailed study of the influence of cross-correlated relaxation on the measurement of $R^Q(D_Z)$ and $R^Q(D_+)$ and derives from the fact that the quadrupolar interaction is dominant.[42] Rather than dwell on this topic further we prefer to illustrate the accuracy of the measured rates by means of a number of validation checks, described below.

Five ^{2}H Relaxation Rates Measured in Protein L are Self-Consistent. All methods described above have been applied to measure relaxation rates in protein L (63 residues) at 500 and 600 MHz (298 K in both cases) and at 600 MHz, 278 K. In addition, measurements have been made on the T22G mutant of the N-terminal SH3 domain from the protein drk (T22G drkN SH3, 59 residues) at 600 MHz, 298 K. This mutant is stabilized relative to the wild-type drkN SH3 domain,[44] and only the folded conformation is observed in solution. In what follows we describe results for protein L recorded at 298 K; all other data can be found in Supporting Information. Figure 4A shows a two-dimensional $^{13}C-^{1}H$ correlation spectrum recorded at 600 MHz using the pulse sequence of Figure 2A ($R^Q(D_+^2)$ measure-

(44) Mok, Y. K.; Elisseeva, E. L.; Davidson, A. R.; Forman-Kay, J. D. *J. Mol. Biol.* **2001**, *307*, 913−28.

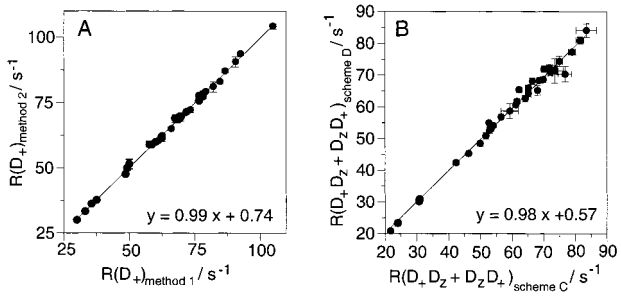

Figure 5. (A) Correlation between $R^Q(D_+)$ obtained by subtraction of $R(I_ZC_Z)$ "on the fly" (*y*-axis) and by subtracting $R(I_ZC_Z)$ from $R(I_ZC_ZD_+)$ in a postacquisition manner (*x*-axis) using rates measured for protein L at 600 MHz, 298 K. (B) Correlation between $R^Q(D_+D_Z + D_ZD_+)$ obtained via methods C and D, Figure 2. In both cases straight lines correspond to the linear regression of the plotted points, with the equations of the best fit lines indicated.

ment) with $T = 1.40$ ms. Experimental decays for the five spin operators described above fitted to monoexponential functions are shown in Figure 4B−E for Ala50, Thr17, Ile4γ, and L56δ2, respectively. Not surprisingly, the operators D_+ and $D_+D_Z + D_ZD_+$ relax much more efficiently than the remaining three, reflecting the fact that the decay rates for only these operators contain $J(0)$ contributions from quadrupolar relaxation. Differences observed between the residues illustrated in the figure reflect varying contributions from internal dynamics.Figure 5A shows the correlation between $R^Q(D_+)$ rates measured using the scheme illustrated in Figure 2, where $R(I_ZC_Z)$ is subtracted "on the fly" (using the additional relaxation delay between *f* and *g* in Figure 2, referred to as method 2), and using our previously published approach where $R(I_ZC_ZD_+)$ and $R(I_ZC_Z)$ are measured in independent experiments and the rates subtracted in a postacquisition manner (method 1). It is clear that the two methods give identical rates to within experimental error estimated on the basis of the signal-to-noise in the experiments. In Figure 5B $R^Q(D_+D_Z + D_ZD_+)$ values obtained using schemes C and D in Figure 2 are shown to be in excellent agreement. Because method C is a factor of 4/3 more sensitive than D (see below), we prefer to use this sequence for measurement of the relaxation of antiphase deuterium magnetization.

Jacobsen and co-workers have shown that the quadrupolar relaxation rates (eqs 1a−e) must fulfill the following inequalities:[31]

$$\frac{5}{3}R^Q(D_+D_Z + D_ZD_+) \geq R^Q(D_+) \geq \frac{5}{3}R^Q(3D_Z{}^2 - 2) \geq \frac{5}{3}R^Q(D_+{}^2) \geq R^Q(D_Z) \quad (12)$$

if $J(0) \geq J(\omega_D) \geq J(2\omega_D)$. Figure 6A shows the five rates multiplied by the coefficients indicated in eq 12 (i.e., 5/3 for three of the five values) as a function of residue for protein L (600 MHz, 298 K). Notably, there are no violations in the inequalities listed above for this data set nor for any data sets that we have obtained at different fields, at different temperatures, or with other proteins.

It is also clear from eqs 1a−e that the five relaxation rates measured at a given static magnetic field depend on a spectral density function evaluated at only three different frequencies. Consequently, a pair of relationships termed *consistency*

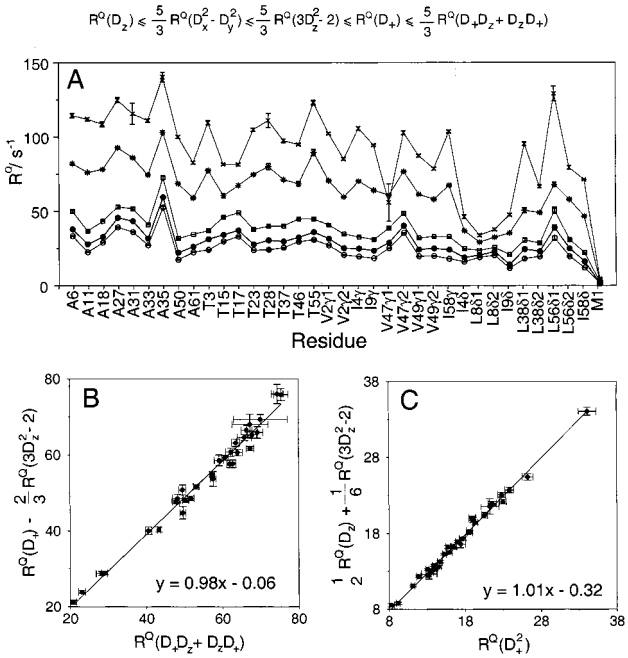

Figure 6. (A) Plot of $R^Q(D_Z)$ (○), $R^Q(D_+)$ (∗), $^5/_3R^Q(3D_Z^2 - 2)$ (□), $^5/_3R^Q(D_+^2)$ (●), and (5/3)$R^Q(D_+D_Z + D_ZD_+)$ (×) as a function of residue in protein L, 298 K, 600 MHz, with the residues ordered according to side-chain length. The rates measured for Met 1 are only approximate because the *T* delays used in experiments are not optimal for this very slowly relaxing residue. (B, C) Consistency relationships, eq 13, evaluated using the five experimentally measured deuterium relaxation rates per methyl group in protein L, 298 K, 600 MHz. Best fit lines are indicated along with their equations.

relationships can be derived. One possible set of relations is[31]

$$R^Q(D_+D_Z + D_ZD_+) = R^Q(D_+) - \frac{2}{3}R^Q(3D_Z{}^2 - 2) \quad (13)$$

$$R^Q(D_+{}^2) = \frac{1}{2}R^Q(D_Z) + \frac{1}{6}R^Q(3D_Z{}^2 - 2)$$

Parts B and C of Figure 6 illustrate the excellent correlation between the rates $R^Q(D_+D_Z + D_ZD_+)$ and $R^Q(D_+{}^2)$ obtained from measurements on protein L at 600 MHz, 298 K and the corresponding values obtained from the linear combinations of measured rates listed on the right-hand side of eq 13. Similar correlations for protein L obtained at 500 MHz, 298 K or at 600 MHz, 278 K or for the T22G drkN SH3 domain, 600 MHz, 298 K are shown in the Supporting Information.

Relative Sensitivity of the Experiments for Measuring the Five ^{2}H Rates. In what follows we consider the sequences of Figure 6 of Muhandiram et al.[18] for measuring ^{2}H longitudinal and transverse relaxation rates as well as the experiments of Figure 2 in this paper for obtaining rates for double quantum, quadrupolar order and antiphase transverse ^{2}H magnetization. Neglecting relaxation for the moment, it can be shown that the relative sensitivities of the experiments are $A_1(D_Z)$:$A_1(D_+)$:$A_2(D_+{}^2)$:$A_2(3D_Z{}^2 - 2)$:$A_2(D_+D_Z + D_ZD_+)_{\text{scheme C}}$:$A_3(D_+D_Z + D_ZD_+)_{\text{scheme D}}$, where $A_1 = 2\sin^2(2\pi J_{CD}\xi)$, $A_2 = (1/2)\{\cos(4\pi J_{CD}(T_C - \tau_C)) - 1\}^2$, and $A_3 = (3/8)\{\cos(4\pi J_{CD}(T_C - \tau_C)) - 1\}^2$ and the subscripts "scheme C" and "scheme D" distinguish between the two sequences (C, D in Figure 2) that can be used for measuring the relaxation of antiphase ^{2}H magnetization. Note that ξ corresponds to τ_C in Figure 6A of ref 18. Setting the delays ξ

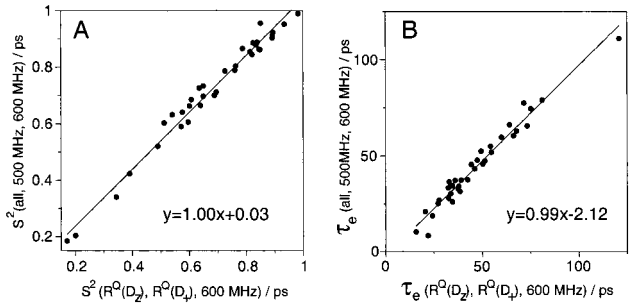

Figure 7. Correlation between motional parameters S_f^2 (A) and τ_f (B) obtained from fits to the Lipari−Szabo model,[38,39] eqs 1 and 2, involving different subsets of experimental data. Parameters extracted from the analysis of all five relaxation rates measured at two static fields (500 and 600 MHz) are plotted along the *y* axis, while those extracted using only $R^Q(D_Z)$ and $R^Q(D_+)$ measured at 600 MHz are plotted along the *x* axis. A value of $\tau_R = 4.05$ ns from ^{15}N relaxation data was employed along with a value of 167 kHz for the quadrupolar constant,[40] e^2qQ/h.

$= 1/4J_{CD}$ and $2T_C - 2\tau_C = 1/2J_{CD}$ for optimal sensitivity it is clear that for $T = 0$ all of the experiments generate spectra of equal signal-to-noise in the absence of relaxation and neglecting pulse imperfections, with the exception of experiment D (Figure 2) which is three-fourths as sensitive. Experimentally we observe, however, that the schemes presented here are roughly a factor of 2−2.5 less sensitive than the corresponding sequences for measuring ^{2}H T_1 and $T_{1\rho}$ relaxation rates. This is a result of the fact that in the present set of experiments (Figure 2) ^{13}C magnetization must evolve for approximately twice as long under the influence of the one-bond ^{13}C−^{2}H scalar coupling interaction, and during this prolonged period ^{2}H spin flips degrade the transfer efficiency. We have been able to obtain high-quality relaxation data with the schemes of Figure 2 for protein L at 278 K, where the overall correlation time is 8 ns; it is likely that the experiments will prove to be of sufficient sensitivity for application to molecules on the order of approximately 150 residues or less. In contrast, the ^{2}H T_1 and $T_{1\rho}$ relaxation schemes presented previously can be applied to larger proteins or protein complexes.[28,45]

Application of Methodology to Protein Studies. All five of the ^{2}H spin relaxation rates have been measured for protein L at 500 and 600 MHz, 298 K, and used to calculate S_f^2 and τ_f values on a per-residue basis, using the simple model-free approach of Lipari and Szabo[38,39] (i.e., assuming that eq 2 is valid). In this analysis a correlation time, τ_R, of 4.05 ns was employed to describe the overall tumbling of the protein, obtained from ^{15}N spin relaxation measurements.[46] Figure 7A illustrates the correlation between order parameters extracted from a best fit to the 10 experimental rates (5 at each field) vs those generated from a fit involving only $R^Q(D_Z)$ and $R^Q(D_+)$ values measured at 600 MHz. A good correlation is found, with a pairwise root mean square deviation value of 3.8%. In Figure 7B the correlation between τ_f values obtained using either 10 or 2 relaxation rates is shown and again good agreement is obtained.

The ability to measure five relaxation rates per methyl site (and more if additional fields are employed) presents an opportunity to go beyond the simple S_f^2, τ_f analysis and to examine in more detail the dynamics at side-chain positions in proteins. The present paper clearly demonstrates that it is possible to measure all five relaxation rates of a single ^{2}H spin in a reliable manner and that these rates are internally consistent. In the following paper in this issue, more complex analyses of side-chain dynamics are considered using new spectral density mapping procedures and more sophisticated models guided by insight provided by a 50 ns molecular dynamics trajectory of the drkN SH3 domain. The effects of both nanosecond time scale local dynamics and anisotropic overall tumbling are also described.

Materials and Methods

All spin relaxation experiments were recorded on a 1.8 mM ^{15}N, ^{13}C, 50% ^{2}H-labeled sample of protein L, 50 mM Na_3PO_4, pH 6.0, 0.05% NaN_3, 10% ^2H_2O that was prepared as described previously[47] or a 1.0 mM sample of ^{15}N, ^{13}C, 50% ^{2}H-labeled Thr22Gly mutant of the N-terminal SH3 domain from the protein drk (50 mM Na_3PO_4, pH 6.0, 10% ^2H_2O), prepared as described by Mittermaier and Kay.[40] Although the ^{15}N label is not required for the measurement of ^{2}H spin relaxation rates, interpretation of the ^{2}H relaxation data using the model-free approach of Lipari and Szabo[38,39] requires knowledge of the overall tumbling time which is readily obtained from ^{15}N spin relaxation experiments (see above). We prefer to record all data on a single sample and therefore prepare protein that is ^{15}N-, ^{13}C-, and ^{2}H-labeled. Stereospecific assignments of the methyl carbons of Val and Leu were obtained by the method of Neri and co-workers[48] using samples that were prepared with a 1:9 mixture of ^{13}C- and ^{12}C-glucose as the sole source of carbon.

Experiments were recorded at 298 K on Varian Inova 600 and 500 MHz spectrometers as complex data matrices comprised of 102 × 576 points (600 MHz) or 84 × 512 points (500 MHz). 16 transients/FID were signal averaged for all experiments recorded at 298 K, with the exception of 32 transients/FID for the sequence of Figure 2D and 8 transients/FID for measuring $R(I_ZC_Z)$, and relaxation delays of between 1.5 and 2 s were employed in each of the data sets. $R^Q(D_Z)$, $R^Q(D_+^2)$, $R^Q(3D_Z^2 - 2)$, and $R(I_ZC_Z)$ rates were recorded with *T* delays (298 K) of 1.4, 3.6, 7.6, 11.8, 16.5, 21.6, 27.4, 33.8 (duplicate), 41.3, and 50 ms, while *T* delays (298 K) of 0.20, 1.5, 3.0, 4.7, 6.6, 8.7, 10.9, 13.5 (duplicate), 16.5, and 20 ms were used for $R^Q(D_+)$ and $R^Q(D_+D_Z + D_ZD_+)$.

All data sets were processed and analyzed with NMRPipe software.[49] Rates were obtained by fitting cross-peak intensities to a single exponential function, as described previously,[18] with errors estimated by Monte Carlo analysis.[50] Average error values of 2.7, 2.7, 3.6, 2.5, and 4.8% were obtained for $R^Q(D_Z)$, $R^Q(D_+)$, $R^Q(3D_Z^2 - 2)$, $R^Q(D_+^2)$, and $R^Q(D_+D_Z + D_ZD_+)$, respectively. Motional parameters, S_f^2 and τ_f, were extracted by minimizing a function of the form $\chi^2 = \sum_i (R_{i,calc}{}^Q - R_{i,exptl}{}^Q)^2/\sigma_i^2$ where $R_{i,calc}{}^Q$ and $R_{i,exptl}{}^Q$ are the calculated and experimental relaxation rates, the index *i* labels each of the independent relaxation rates measured and σ_i is the estimate of the error in the experimental rate. Expressions for $R_{i,calc}{}^Q$ were obtained from eq 1 using the form of spectral density defined by eq 2. Note that α values of 1/9 for the quadrupolar and intra-methyl C−D dipolar interactions, 1/4 for intra-

(45) Ishima, R.; Louis, J. M.; Torchia, D. A. *J. Mol. Biol.* **2001**, *305*, 515−21.
(46) Farrow, N. A.; Muhandiram, R.; Singer, A. U.; Pascal, S. M.; Kay, C. M.; Gish, G.; Shoelson, S. E.; Pawson, T.; Forman-Kay, J. D.; Kay, L. E. *Biochemistry* **1994**, *33*, 5984−6003.
(47) Mittermaier, A.; Kay, L. E. *J. Am. Chem. Soc.* **2001**, *123*, 6892−903.
(48) Neri, D.; Szyperski, T.; Otting, G.; Senn, H.; Wüthrich, K. *Biochemistry* **1989**, *28*, 7510−7516.
(49) Delaglio, F.; Grzesiek, S.; Vuister, G. W.; Zhu, G.; Pfeifer, J.; Bax, A. *J. Biomol. NMR* **1995**, *6*, 277−293.
(50) Kamith, U.; Shriver, J. W. *J. Biol. Chem.* **1989**, *264*, 5586−5592.
(51) Geen, H.; Freeman, R. *J. Magn. Reson.* **1991**, *93*, 93−141.
(52) Patt, S. L. *J. Magn. Reson.* **1992**, *96*, 94−102.
(53) Boyd, J.; Soffe, N. *J. Magn. Reson.* **1989**, *85*, 406−413.
(54) McCoy, M. A.; Mueller, L. *J. Am. Chem. Soc.* **1992**, *114*, 2108−2112.
(55) Shaka, A. J.; Keeler, J.; Frenkiel, T.; Freeman, R. *J. Magn. Reson.* **1983**, *52*, 335−338.
(56) Marion, D.; Ikura, M.; Tschudin, R.; Bax, A. *J. Magn. Reson.* **1989**, *85*, 393−399.

Table 1. Coefficients, a_q, for the Dipolar Contributions to the Relaxation of the Spin Operators of Interest[a]

			I_ZC_Z					$I_ZC_ZD_Z$				
A	B	α	J(0)	$J(\omega_A-\omega_B)$	$J(\omega_A)$	$J(\omega_B)$	$J(\omega_A+\omega_B)$	J(0)	$J(\omega_A-\omega_B)$	$J(\omega_A)$	$J(\omega_B)$	$J(\omega_A+\omega_B)$
C	D	1/9		8/3	8		16		1	12	3	6
I^i and I^j	C	1/9		1	3	6	6		1	3	6	6
I^i and I^j	D	1/4		8/3	8		16		2	12	6	12
I^i	I^j	1/4			3		12			3		12
D	I^k	∼1							1	3		6
I^i and I^j	I^k	∼1		1	3		6		1	3		6
C	C′	1		1	3		6		1	3		6

			$I_ZC_ZD_+$					$I_ZC_ZD_+^2$				
A	B	α	J(0)	$J(\omega_A-\omega_B)$	$J(\omega_A)$	$J(\omega_B)$	$J(\omega_A+\omega_B)$	J(0)	$J(\omega_A-\omega_B)$	$J(\omega_A)$	$J(\omega_B)$	$J(\omega_A+\omega_B)$
C	D	1/9	2	5/2	3	3/2	15	8	1		3	6
I^i and I^j	C	1/9		1	3	6	6		1	3	6	6
$I^i$and I^j	D	1/4	4	3	6	3	18	16	2	12	6	12
I^i	I^j	1/4			3		12			3		12
D	I^k	∼1	2	1/2	3/2	3	3	8	1	3	12	6
I^i and I^j	I^k	∼1		1	3		6		1	3		6
C	C′	1		1	3		6		1	3		6

			$I_ZC_Z(2D_Z^2-1)$					$I_ZC_Z(D_+D_Z+D_ZD_+)$				
A	B	α	J(0)	$J(\omega_A-\omega_B)$	$J(\omega_A)$	$J(\omega_B)$	$J(\omega_A+\omega_B)$	J(0)	$J(\omega_A-\omega_B)$	$J(\omega_A)$	$J(\omega_B)$	$J(\omega_A+\omega_B)$
C	D	1/9			8	8		2	1/2	3	15/2	3
I^i and I^j	C	1/9		1	3	6	6		1	3	6	6
I^i and I^j	D	1/4		8/3	8	16	16	4	3	6	15	18
I^i	I^j	1/4			3		12			3		12
D	I^k	∼1		8/3	8		16	2	5/2	15/2	3	15
I^i and I^j	I^k	∼1		1	3		6		1	3		6
C	C′	1		1	3		6		1	3		6

[a] Autocorrelated relaxation contributions originating from dipolar interaction $H^D(AB)$. When spin A represents two protons, I^i and I^j, the listed contribution is the sum of autocorrelated terms corresponding to $H^D(I^iB)$ and $H^D(I^jB)$. Spin operator I_Z is $I_Z = I_Z{}^i + I_Z{}^j$. The operator $I_ZC_Z(2D_Z{}^2 - 1)$ is equivalent to $I_ZC_Z(2D_Z{}^2 - E)$, where E is the spin 1 operator identity.

methyl I−D interactions, and 1 for dipolar interactions involving proximal protons *k* outside the methyl group, have been used.

Acknowledgment. The authors thank Tony Mittermaier (University of Toronto) for preparation of the samples used in the study, Dr. D. A. Torchia (NIH, Bethesda, MD) for many helpful discussions and for suggesting to record the relaxation of antiphase deuterium magnetization, and Dr. Debbie Mattiello and Mark Van Creigen, Varian, for help with setting up the experiments at 400 MHz at Varian, Palo Alto, CA. O.M. and N.R.S. acknowledge funding from the Ministerio de Educacion y Cultura (MEC) (O.M.) and the Canadian Institutes of Health Research (CIHR) in the form of a Centennial Fellowship (N.R.S.). This work is supported by grants from the Natural Sciences and Engineering Research Council of Canada and the CIHR. L.E.K. is a foreign investigator of the Howard Hughes Medical Research Institute.

Appendix: Contributions from Dipolar Interactions to Autorelaxation of the Operators, I_ZC_Z, $I_ZC_ZD_Z$, $I_ZC_ZD_+$, $I_ZC_Z(2D_Z^2 - 1)$, $I_ZC_Z(D_+D_Z + D_ZD_+)$, and $I_ZC_ZD_+^2$

Starting from eq 8 the dipolar contributions to the relaxation of spin A from spin B can be calculated according to

$$R_{AB}^D = \left(\frac{1}{10}\right)\left(\frac{\mu_o}{4\pi}\right)^2 \frac{\gamma_A{}^2\gamma_B{}^2\hbar^2}{\langle r_{AB}{}^3\rangle^2} \sum_q a_q J_{AB}(\omega_q) \qquad (14)$$

where γ_A and γ_B are the gyromagnetic ratios of the nuclei A and B, h is Plank's constant, $\hbar = h/2\pi$, r_{AB} is the distance between the two nuclei, and $J_{AB}(\omega_q)$ is a spectral density function given by eq 2. The coefficients a_q are presented in Table 1. Spins A and B are identified with the two particular nuclei involved in each dipolar interaction, with the nuclei considered in the analysis shown in Figure 3. The value of the geometrical factor α (see eq 2 and Materials and Methods) is also reported in the table for each different pair of nuclei. For example, to calculate the contribution to the relaxation of the operator $I_ZC_Z(2D_Z^2 - 1)$ from the dipolar interaction between methyl spins C and D, the coefficients, $a_q = 0$, 0, 8, 8, and 0 for the spectral density terms $J(0)$, $J(\omega_C-\omega_D)$, $J(\omega_C)$, $J(\omega_D)$, and $J(\omega_C+\omega_D)$ respectively, are obtained directly from the table. The geometrical factor α, also obtained from the table, is equal to 1/9 so that substitution into eq 14 gives the following expression for the dipolar relaxation term:

$$R_{CD}^D(2D_Z{}^2 - 1) = \left(\frac{1}{10}\right)\left(\frac{\mu_o}{4\pi}\right)^2 \frac{\gamma_C{}^2\gamma_D{}^2\hbar^2}{\langle r_{CD}{}^3\rangle^2} [8J(\omega_C) + 8J(\omega_D)] \qquad (15)$$

with an expression for the spectral density function given by

$$J(\omega_q) = \frac{1}{9} S_f{}^2 \frac{\tau_R}{1 + (\omega_q\tau_R)^2} + \left(1 - \frac{1}{9}S_f{}^2\right)\frac{\tau}{1 + (\omega_q\tau)^2} \qquad (16)$$

For each term in eq 8 the contribution to the relaxation of the operator of interest is calculated and the net rate, ρ, given by the sum of the individual contributions, is determined. Consequently, for each of the six operators $I_ZC_ZD_v$ from Table 1 we obtain

$$\frac{d}{dt} I_Z C_Z D_v = -\rho_v I_Z C_Z D_v \quad (17)$$

where $I_Z = I_Z{}^i + I_Z{}^j$. In principle, auto- and cross-correlated cross-relaxation terms must also be included in eq 17. Simulations establish, however, that the effects of such terms are negligible for the values of T that are employed in the experiments of Figure 2.

Supporting Information Available: Figures analogous to Figure 6 illustrating the consistency of the ^{2}H relaxation data measured on protein L, 500 MHz, 298 K and 600 MHz, 278 K and on the T22G drkN SH3 domain, 600 MHz, 298 K (PDF). This material is available free of charge via the Internet at http://acs.pubs.org.

JA012497Y